Laser Temperature Jump Study of the Helix⇌Coil Kinetics of an Alanine Peptide Interpreted with a 'Kinetic Zipper' Model

Peggy A. Thompson, William A. Eaton, and James Hofrichter*

Laboratory of Chemical Physics, Building 5, National Institute of Diabetes and Digestive and Kidney Diseases, National Institutes of Health, Bethesda, Maryland 20892-0520

Received February 28, 1997; Revised Manuscript Received May 16, 1997[⊗]

ABSTRACT: The kinetics of the helix⇌coil transition of an alanine-based peptide following a laser-induced temperature jump were monitored by the fluorescence of an N-terminal probe, 4-(methylamino)benzoic acid (MABA). This probe forms a peptide hydrogen bond to the helix backbone, which changes its fluorescence quantum yield. The MABA fluorescence intensity decreases in a single exponential relaxation, with relaxation times that are weakly temperature dependent, exhibiting a maximum value of ∼20 ns near the midpoint of the melting transition. We have developed a new model, the kinetic version of the equilibrium 'zipper' model for helix⇌coil transitions to explain these results. In this 'kinetic zipper' model, an enormous reduction in the number of possible species results from the assumption that each molecule contains either no helical residues or a single contiguous region of helix (the single-sequence approximation). The decay of the fraction of N-terminal residues that are helical, calculated from numerical solutions of the kinetic equations which describe the model, can be approximately described by two exponential relaxations having comparable amplitudes. The shorter relaxation time results from rapid unzipping (and zipping) of the helix ends in response to the temperature jump, while the longer relaxation time results from equilibration of helix-containing and non-helix-containing structures by passage over the nucleation free energy barrier. The decay of the average helix content is dominated by the slower process. The model therefore explains the experimental observation that relaxation for the N-terminal fluorescent probe is ∼8-fold faster than that for the infrared probe of Williams *et al.* [(1996) *Biochemistry 35,* 691−697], which measures the average helix content, but does not account for the absence of observable amplitude for the slow relaxation in the fluorescence experiments (<10% slow phase). If we assume that the activation barrier for the *coil→helix* rate is purely entropic, the model can also explain the maximum in the temperature dependence of the relaxation time for the fluorescent probe. Parameters that best reproduce the melting curves and the ratio of relaxation times predict a value of the cooperativity parameter σ which is ∼3-fold larger than previously reported values obtained from fitting equilibrium data only. The helix growth rate of $\sim 10^8$ s^{-1} that reproduces the experimental relaxation times is ∼100-fold slower than those observed in molecular dynamics simulations. These parameters can be used to simulate the kinetically cooperative formation of a helix from the all-coil state.

Although the helix⇌coil transition has been extensively studied for short, helix-forming peptides at equilibrium, there is remarkably little kinetic information on these molecules. In the classical picture of α-helix formation, two elementary processes occur. The helix first nucleates by forming a single turn, resulting in the formation of a hydrogen bond between the carbonyl of one residue of the nascent helix and the amide N−H of another, displaced four residues toward the C-terminus (*2*, *3*). The helix can then propagate in either direction by the addition of single residues to either end. The equilibrium constants for nucleus formation and propagation are conventionally called σs, and *s*, respectively (see ref 4 for a comprehensive discussion of the competing thermodynamic descriptions of helix⇌coil transitions). For short alanine-based peptides of length 15−20 residues, reported values for σ range from 0.001 to 0.004, and the value of *s* decreases from 2 at low temperatures (∼275 K) to about 1 at high temperature (∼360 K) (*5*−*7*). The free energy barrier for nucleation is therefore ∼4 kcal/mol, and the most favorable free energy for helix propagation is only ∼0.4 kcal/mol. From these numbers, it is easy to see that at least 10 residues are required to make a stable helix; at the midpoint of the transition, the average length of a helix in an infinite poly-α-amino acid is equal to $\sigma^{-1/2}$ (*3*, *8*), that is 15−30 residues.

There are a number of reasons why one would like to understand the kinetics of helix⇌coil transitions in detail. First, the propagation step is arguably the simplest kinetic process that can occur in the folding of a protein. Knowing what determines the rate of this process could provide a key to understanding those that are more complex, since the basic ingredient, which is the loss of conformational entropy required to approach the transition state from the coil state, is common to any elementary step that occurs during protein folding. There has been, to our knowledge, no experiment that measures this rate directly, much less its dependence on temperature or solution conditions. The available estimates have been derived from relaxation data and require prior knowledge of σ to extract the propagation rate (*9*). Second, helix nucleation, which can be viewed as an elementary example of loop formation, may provide some insight into the rates that other elementary structures such as β turns and other tight loops form. Third, because helix

* Author to whom correspondence should be addressed.
[⊗] Abstract published in *Advance ACS Abstracts,* July 1, 1997.

S0006-2960(97)00476-5

formation and melting are among the most rapid cooperative events in folding, these processes can currently be explored by all atom molecular dynamics (MD) simulations (*10*−*13*). A direct comparison of experimental data and simulations will provide a critical test of the validity of the complete classical description of the process embodied in the MD simulations.

Beginning in the mid-1960s, helix⇌coil kinetics of long polypeptides and model compounds were investigated using dispersion techniques, probed either by dielectric loss (*14*) or ultrasonic absorption (*9, 15*−*19*) as well as by conventional temperature-jump (*20*) and electric-field jump (*21, 22*) experiments. The results of a number of these experiments have been summarized by Gruenewald *et al*. (*23*). The maximum relaxation times (observed near the midpoint of the transition) range from 50 ns for poly-γ-benzyl-L-aspartate (*19*) to a few microseconds for poly-L-glutamic acid in water (*20, 21*). These experiments have significant limitations if the objective is to understand the kinetics of helix formation in protein folding. First, the experiments were carried out on homopolymers of high molecular weight. This was done, in part, to decrease the rate of rotational diffusion to the point where it did not complicate the observation of helix⇌coil kinetics. Since globular proteins contain only short helices and are not homopolymers, it is not clear that these results can be applied to protein folding. Second, the experiments are indirect and difficult to interpret quantitatively. The experimental relaxation times are highly system- and solvent-dependent. Nonetheless, these studies remained the only available experimental description of helix⇌coil kinetics until very recently, when new techniques and materials became available to probe this reaction.

The theoretical foundation for interpreting the experiments on helix⇌coil kinetics developed contemporaneously with the early experimental results. The initial rate at which the average helix content of a sequence changes in response to a physical perturbation was first treated by Schwarz (*9*). This basic treatment was expanded by Poland and Scheraga (*24*) to include a larger set of possible transitions. Neither analysis considered the detailed kinetic form of the transition, which was first discussed by McQuarrie *et al*. (*25*) (in the limit where the steps are irreversible) and Gō (*26*) (in the limit where the rate equations can be linearized).

Renewed interest in the kinetics of helix⇌coil transitions has been sparked by three recent developments—the detailed experimental characterization of short peptides that can be thermally melted in aqueous solution (*7, 27*), the availability of modern laser temperature-jump instrumentation (*1, 28*−*32*), and the ability to explore these kinetic processes using all atom MD simulations (*10*−*13, 33*). Modern techniques for peptide synthesis, together with residue-specific probes for helical conformations, have produced a detailed picture of the factors that stabilize the helical conformations of short peptides (*6, 7, 27, 34, 35*). In addition to the well-established intrinsic propensities of specific amino acids for helix formation, these include the presence of specific interactions that can stabilize helix ends (capping) (*34*) and specific hydrophobic and electrostatic interactions between residues in the helical sequence (*27, 35*).

The use of temperature jumps produced by absorption of short laser pulses to study rapid reactions has been under development for more than 25 years. Early attempts utilized dyes to absorb Q-switched pulses from ruby and Nd:glass lasers, providing radiation at 694 and 1060 nm, respectively, and succeeded in producing temperature jumps of ∼4 K (*36, 37*). Temperature jumps produced by direct absorption of near-infrared pulses by water were first described by Turner *et al*. (*38, 39*). The exciting laser pulse at 1.41 μm was generated by Raman-shifting the Nd:YAG fundamental in liquid N_2. Williams *et al*. (*40*) expanded this method by using methane gas to Raman shift Nd:YAG laser pulses (1064 nm) to 1.54 μm. This approach has recently been applied to peptides and proteins by several groups. Williams *et al*. (*1*) used a Nd:YAG-pumped dye laser and generated a ∼7-ns infrared pulse at 2.0 μm by difference mixing in a $LiNbO_3$ crystal. Using infrared detection to measure amide I resonances (1630−1660 cm^{-1}) they observed a relaxation time of 160 ns for the decrease in the average helical content of a 21-residue alanine-based peptide (see Figure 1) after an 18 K temperature jump. This technique has also been used to study the unfolding of apomyoglobin (*30*). The temperature-induced *folding* of apomyoglobin, which can be partially cold denatured at temperatures near 275 K, has been studied by Ballew *et al*. (*31*) by heating with 10-ns pulses at 1.54 μm (*40*) and monitoring tryptophan fluorescence intensities and lifetimes. Phillips *et al*. (*32*) have used still another approach in studies of the unfolding of RNase A by picosecond transient infrared spectroscopy. In this experiment a ∼7-ps Nd:YAG laser pulse (at 532 nm) was absorbed by dye molecules (cresyl violet) that subsequently relaxed to release the photon energy as heat, producing a temperature jump of 3−6 K within 70 ps.

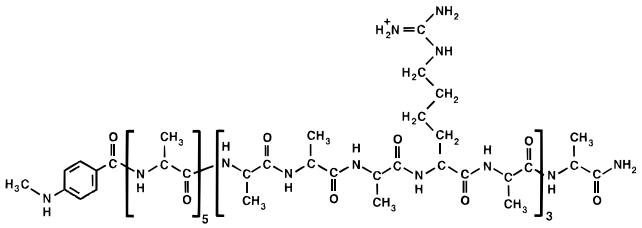

FIGURE 1: Structure of the MABA-labeled peptide. In the helical conformation, the carbonyl oxygen of MABA is hydrogen bonded to the amide nitrogen of the fourth alanine in the peptide.

Within the past 5 years it has also become feasible to explore the dynamics of helix⇌coil transitions using all-atom molecular dynamics simulations. Simulations of helix melting have provided detailed information on the kinetics of the redistribution of hydrogen bonds, of coil nucleation (*hhh*→*hch*), as well as some information on the rate of unzipping of helices (*12*). These results provide a clear example of the enormous wealth of information provided by such simulations. Free energy perturbation studies have also provided information on the free energy barriers encountered in the formation of amide hydrogen bonds (*41*). These results prompted an exploration of helix⇌coil kinetics using a simple sequential nucleation and growth model (*42*). This model did not include statistical factors, (e.g., the large degeneracy in the number of ways short helical sequences can form). These factors are critical to the description of both the equilibrium distribution of helix lengths and the kinetics of the helix⇌coil transition, in particular the rate of helix nucleation. For example, if σs is 0.01, but the peptide can form the first loop of helix at any of 20

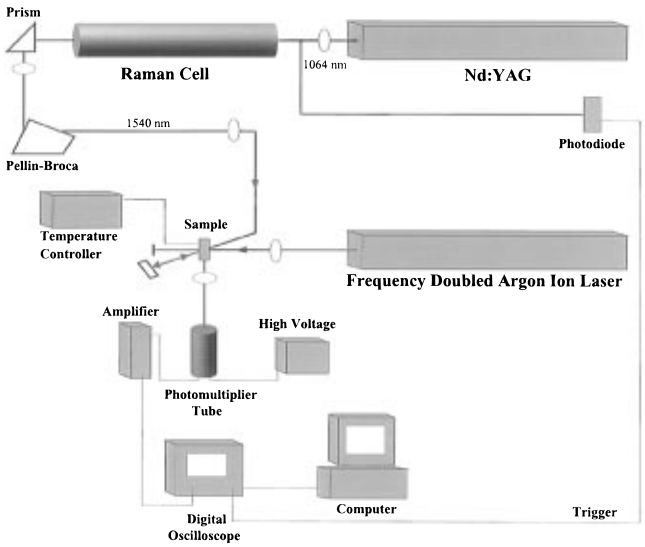

FIGURE 2: Schematic of the laser temperature-jump instrument. See text for description.

sites, the relative probability of a single *h* state is 0.2 rather than 0.01, and the rate of helix nucleation is only 5 (rather than 100) times slower than the rate of propagation.

In this paper, we describe a nanosecond laser temperature-jump apparatus that can monitor changes in either the optical absorption or fluorescence of the sample. We have used this instrument to study a peptide labeled at the N-terminus with the fluorescent probe 4-(methylamino)benzoic acid (MABA). In this peptide, shown in Figure 1, MABA is covalently coupled to the N-terminus of the peptide, forming an additional amide residue; 2D NOESY NMR experiments have shown that the carbonyl oxygen of MABA is hydrogen bonded to the amide nitrogen of the fourth residue when the peptide is in its α-helical conformation (*43*). To interpret this experiment, we have developed the 'kinetic zipper' model for helix⇌coil kinetics which incorporates the single-sequence approximation used in the equilibrium zipper model (*2, 8*).

MATERIALS AND METHODS

Temperature jumps of 10−20 K were generated by absorption of a near-infrared laser pulse at 1.54 μm by the aqueous peptide solution. To measure the kinetics, a continuous ultraviolet probe beam was used to excite the fluorescence of the labeled peptide, and the emitted light was monitored by a photomultiplier. A schematic of the instrument is shown in Figure 2. To produce the temperature-jump pulse, the fundamental (1064 nm) of a Nd:YAG laser (Surelite I, Continuum, Santa Clara, CA), operating at 1.67 Hz, was focused with a 0.75-m lens into a 1 m Raman cell (Princeton Optics, Princeton NJ). The Raman cell contained 600 psi of CH_4 and 500 psi of He and had a conversion efficiency of ∼20% for the first Stokes line (1.54 μm). This wavelength falls in a near-IR absorption band (an OH stretching overtone) of water, with an extinction coefficient of $\epsilon = 5.2$ cm^{-1}. The 1.54-μm light pulse (∼4 ns full width at half-maximum (fwhm)) was separated from the fundamental and anti-Stokes lines with a Pellin−Broca prism and focused onto the sample by a 0.75-m lens to give a spot size of ∼1 mm. Using a 500-μm pathlength cuvette, ∼40% of the infrared beam is absorbed. To ensure uniform heating at the front and back of the cuvette, the remaining

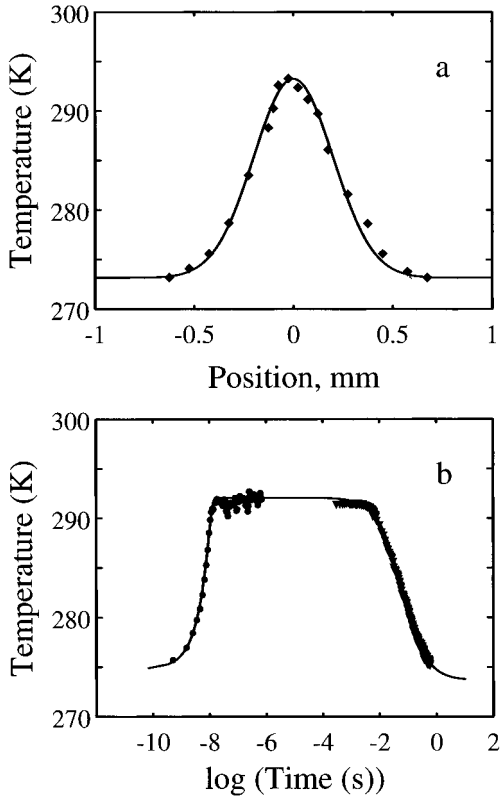

FIGURE 3: Position and time dependence of the fluorescence intensity of tryptophan observed during temperature jumps from 273 to 293 K. (a) Spatial profile of temperature pulse. The fitted half-width is 0.49 mm. (b) Temporal profile of the temperature pulse. The rise in fluorescence intensity has been fitted with the convolution of the square of a gaussian pulse, having a half width of 12 ns. It can alternatively be fitted with an exponential having a 5 ns time constant (the approximate time resolution of the instrument). The decay of the temperature pulse is fitted with the function: $T(t) = 273.65 + 1.13/(0.0612 + t)$, giving the half-time for the decay as 61 ms, and a decay time for the temperature to decrease by 1/10 of the total temperature increase as ∼5 ms. Relaxation kinetics over a 6-decade time window, extending from ∼5 ns to ∼5 ms, can thus be measured with this instrument.

60% of the 1.54-μm light was reflected back onto the sample in a double-pass configuration. The absorbed radiation directly heats a small volume of water by vibrational excitation. From the measured cross section of the heated volume, shown in Figure 3a, the width at half height is ∼0.5 mm, so the heated volume is ∼0.1 μL. The temperature profile is constant over about the central 100 μm of the heated spot.

The ultraviolet beam used to excite MABA fluorescence was generated with an intracavity frequency-doubled argon ion laser (FRED, Coherent, Palo Alto, CA) operating at 264 nm. The beam was focused onto the region of constant temperature by a lens having a 10-cm focal length, producing a spot size of 60−70 μm. For fluorescence experiments, a front-face illumination geometry was used. The emitted light was collected at 90° to the excitation beam by a 3.9-cm focal length lens, filtered from residual reflected excitation and infrared light, and detected with a photomultiplier tube (1P28, Hamamatsu, Bridgewater, NJ). The signal was amplified by cascading two channels (5× gain per channel) of a fast preamp module (Model SR240; Stanford Research Systems, Sunnyvale, CA) and digitized and averaged using a digital oscilloscope (TDS 620; Tektronix, Medford, OR). The waveforms from the oscilloscope were transferred to a

personal computer for analysis.

The size of the laser temperature jump was characterized by monitoring changes in tryptophan fluorescence, the intensity of which decreases ~1% for each 1 K increase in temperature. Temperature jumps of 20 K can be generated using 1.54-μm pulse energies of ~10 mJ. Since the vibrational relaxation time of water is about 10^{-11} s (*44*, *45*), the time required to reach the higher temperature is determined by the laser pulse width. Figure 3b shows that a temperature jump from 273 to 293 K occurs in ~5 ns and that the heated volume does not begin to cool by thermal diffusion for several milliseconds. This provides a dynamic range of more than 6 decades of time ($\sim 10^{-8} - \gtrsim 10^{-3}$ s) in which to explore the kinetics.

The peptide (Figure 1) was donated by Peter Kim. As determined from HPLC, its purity was greater than 90%. Steady-state fluorescence emission spectra of this peptide were collected from 310 to 480 nm using an SLM 8000 spectrofluorimeter. The excitation wavelength in both equilibrium and kinetic experiments was 264 nm. A 1 × 1 cm pathlength cuvette was used with concentrations of ~9 μM. The emission quantum yields were determined relative to *N*-acetyl-L-tryptophanamide (Sigma, Saint Louis, MO) at pH = 6.9 ($\Phi_f = 0.13$) (*46*). Circular dichroism spectra were measured on a JASCO 710 spectropolarimeter (JASCO, Easton, MD) using a 0.5-mm pathlength cylindrical cell and concentrations of ~0.26 mM. Peptide concentrations were determined from the absorbance of the MABA moiety at 298 nm using an extinction coefficient of 14 300 ± 700 M^{-1} cm^{-1}, determined gravimetrically for MABA (Aldrich, Milwaukee, WI). The kinetic experiments were carried out in a 0.05 × 1.0 cm fluorescence cuvette (NSG Precision Cells, Farmingdale, NY) at concentrations of ~0.5 mM. The melting reaction was monitored by detecting the fluorescence intensity change of the MABA-labeled peptide for the wavelength range 320−400 nm.

Kinetic simulations and analysis were carried out using Matlab (The Mathworks, Natick, MA). For convenience and to permit comparison with the simple, sequential model (*42*), the matrix was laid out in blocks, with each block corresponding to a different position for the first helical residue. The matrix then has the form

$$\begin{pmatrix} [\text{all coil}] & & & \\ & [h_1 = 1]\ (n \times n) & & \\ & & [h_1 = 2]\ (n-1 \times n-1) & \\ & & \cdots\cdots & \\ & & & [h_1 = n-1]\ (2 \times 2) \\ & & & [h_1 = n]\ (1 \times 1) \end{pmatrix} \quad (1)$$

where each subblock describes helix propagation from a fixed initial site, h_1. The two subblocks in the upper left corner describe the linear, sequential model described by Brooks (*42*). The matrix is sparse because connections only exist between adjacent blocks. For example, the $[h_1 = i]$ block can add a helical residue at position $i - 1$ and produce a species in the $[h_1 = i - 1]$ block or remove a helical residue at position i to produce a species in the $[h_1 = i + 1]$ block. In addition, each block is connected to the all-coil state by the nucleation rate, σk_+ and by k_-. These simple rules make it straightforward to generate the rate matrix in the general case, by generating the appropriate off-diagonal elements of the subblocks as well as the set of connecting elements as vectors. The diagonal elements can then be produced by summing the off-diagonal elements for each column. The matrix was diagonalized by a standard eigenvalue analysis.

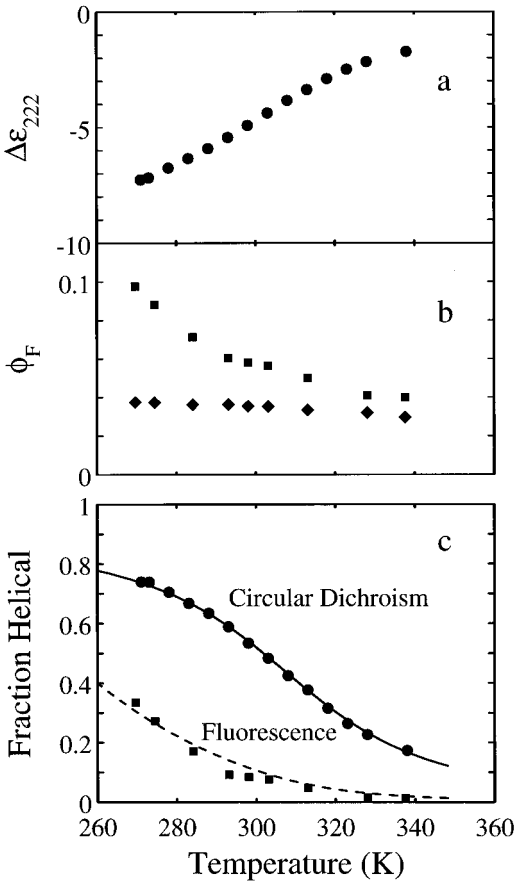

FIGURE 4: Equilibrium data for the MABA peptide as a function of temperature. (a) (●) Circular dichroism at 222 nm. (b) (■) Fluorescence quantum yield of the MABA peptide and (♦) free MABA in solution. (c) (—) Fit of the average fraction of helical residues to the CD data using the single-sequence approximation. The fraction helix is plotted as a function of temperature. The parameters obtained from the fit are $s_0 = 1.482$ and $\sigma = 0.00117$. ΔH_s was assumed to have a value of −1.3 kcal/mol residue, as determined by Scholtz *et al*. (*5*). A comparably good fit was obtained using $\Delta H_s = -1.5$ kcal/mol residue, yielding $s_0 = 1.525$ and $\sigma = 0.025$. (●) The MABA peptide CD data in (a) scaled as required by the fit. (– –) The N-terminal helix probability calculated from the model. (■) The MABA peptide fluorescence data in (b) scaled to best fit the calculated values.

RESULTS AND DISCUSSION

Characterization of the Helix⇌Coil Transition. The equilibrium properties of the peptide were characterized by circular dichroism and fluorescence measurements. At low temperatures, the CD spectrum has the characteristic double minima at 222 and 208 nm indicative of an α-helix. An isodichroic point is observed at 202 nm, suggesting that there is no significant population of conformations that are neither α-helical nor random coil. The circular dichrioism ($\epsilon_l - \epsilon_r$) at the 222-nm minimum, $\Delta\epsilon_{222}$, is shown in Figure 4a. As observed for other small helical peptides (*5*, *47*, *48*), the transition is very broad, extending over more than 70 K. Because all amino acids in the peptide contribute to the CD signal, the helical fraction as determined by $\Delta\epsilon_{222}$ measures the average helical content [perhaps with some bias toward the central residues of a helical sequence (*48*−*50*)]. If the

helix content is estimated from the CD alone (*48, 49*), the maximum helix content is about 80%. We also fitted the CD using the single-sequence approximation (see below) permitting the overall fraction of helix to be scaled in the fit. The best fit located the midpoint of the folding curve at 303 K and also suggests that at 273 K the peptide is ~75% α-helical (Figure 4c).

In marked contrast to free MABA in solution, the total fluorescence intensity for MABA bound to the peptide is strongly dependent on temperature, decreasing 55% as the temperature increases from 275 to 340 K (Figure 4b). It is reasonable to assume that the MABA fluorescence is sensitive only to the conformation of the N-terminal amino acid residues since this is the location of the fluorescent probe and there are no other chromophores in the peptide that can quench the fluorescence via a Forster mechanism. It has been shown that carbonyl groups are efficient quenchers of both tryptophan and tyrosine fluorescence (*51, 52*). The large increase in the quantum yield of tyrosine that accompanies the folding of the α-helical proteins paramyosin and tropomyosin has been attributed to a decrease in the quenching efficiency of the backbone carbonyl when it is hydrogen bonded in the α-helix (*53*). It is likely that the formation of the helical hydrogen bond has a similar effect on the fluorescence of MABA. We therefore conclude that the fluorescence intensity for the MABA peptide acts as a probe for the conformation of the N-terminus of the peptide.[1] Comparison of the fluorescence quantum yields and the CD data (Figure 4c) shows pronounced differences in the apparent melting curves. Since CD measures the average helix content and the MABA fluorescence is sensitive to the N-terminal helix content, one would anticipate that these two probes would respond differently to parameters that affect helix stability. This expectation is borne out in the modeling discussed below.

Laser temperature jumps were used to rapidly perturb the helix⇌coil equilibrium at temperatures ranging from 270 to 325 K. Figure 5 shows examples of the kinetics measured for jumps to final temperatures of 275, 293, and 319 K. All of the relaxation data could be fitted with a single exponential decay. The relaxation time at 293 K, near the midpoint of the melting transition, is somewhat longer than that observed at both the higher and lower temperatures. It is important to note that the pre-jump amplitudes do not differ significantly from the initial amplitudes obtained from the exponential fits to the data. This result shows that there are no substantially faster processes that alter the fluorescence quantum yield of the MABA probe. The dependence of the measured relaxation rates on temperature is shown in Figure 6. The relaxation rates show a minimum near 305 K and increase by more than a factor of 2 at both 280 and 330 K. If we compare these results with those of Williams *et al.* (*1*) on the same (but not MABA-labeled) peptide (Figure 6), we find that their reported relaxation rate is approximately

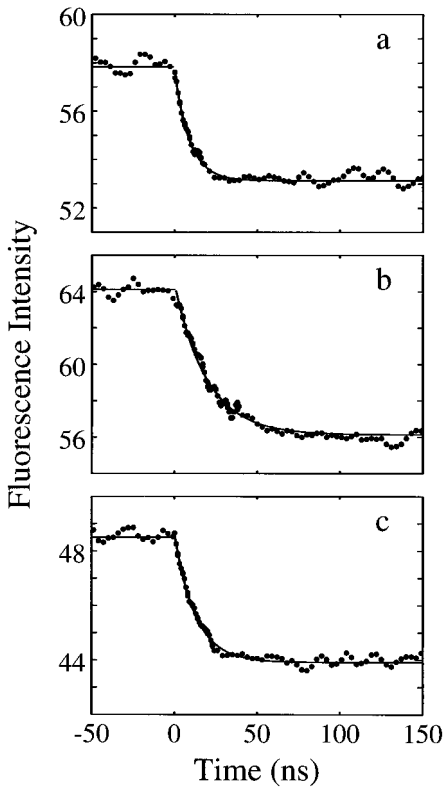

FIGURE 5: Kinetics for the change in fluorescence of the MABA peptide. Data are shown for temperature jumps (a) from 265 to 275 K, (b) from 273 to 293 K, and (c) from 303 to 319 K. Intensity is plotted in arbitrary units. (—) Fits to the data with a single exponential relaxation. The relaxation rates obtained from the fits were (a) 1.14×10^8 s^{-1}; (b) 5.0×10^7 s^{-1}; and (c) 8.1×10^7 s^{-1}.

8 times smaller than those we have observed under similar conditions.

Kinetic Modeling. There are two principal experimental results that need to be explained. The first is the fact that significantly different rates are obtained if one measures the time dependence of forming the N-terminal hydrogen bond, probed by MABA, than for the average helical population, probed by the infrared absorption of the amide I bands. The second is that the rate observed in the fluorescence experiments is nearly temperature independent and, in fact, exhibits a weak minimum near the midpoint of the melting curve.[2]

To address these questions, we needed to find a model for the kinetics of the helix⇌coil transition that incorporated the major kinetic features of the process and also provided a sufficiently accurate description of the thermodynamics so that it could be used to simultaneously model kinetic and equilibrium data. We chose a model which we call the 'kinetic zipper' model because it is the kinetic version of the equilibrium zipper model, first described by Schellman (*2*). In this model, residues can adopt only two conforma-

[1] Two additional observations support the conclusion that the hydrogen bonding of the MABA carbonyl to the amide nitrogen is responsible for the increase in fluorescence. First, adding 22% trifluoroethanol, which is expected to increase the helical content of the peptide, produces nearly a 3-fold increase in the fluorescence. Second, the fluorescence of free MABA increases upon addition of urea, which presumably results from hydrogen bonding of the MABA carbonyl to the amino nitrogens.

[2] In classical kinetic theory for long helices (*9*), which assumes only small perturbations, similar behavior is predicted. The initial response of the system is characterized by the relaxation time τ^* where

$$\frac{1}{\tau^*} = k_+\{(s-1)^2 + 4\sigma\}$$

If σ and k_+ have a small temperature dependence, this analysis predicts a maximum value of τ^* ($= (4k_+\sigma)^{-1}$) near the midpoint of the transition, i.e., $s \approx 1$. This model, however, applies only to the average helical residue (end effects are assumed to be negligible). The classical theory cannot therefore be applied to our experiments that monitor helix content *only* near the N-terminus.

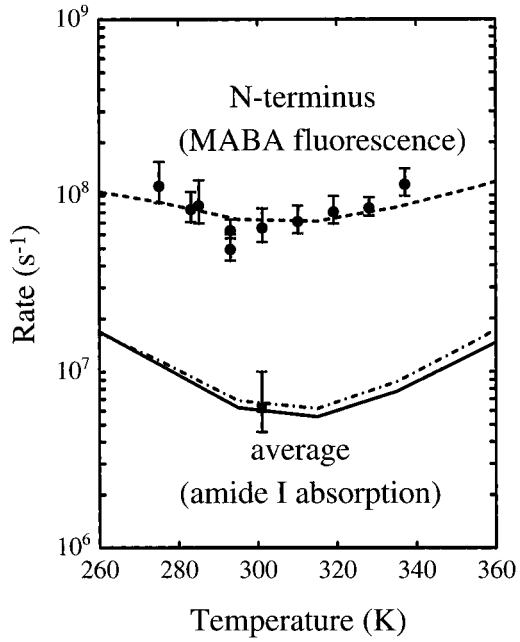

FIGURE 6: Temperature dependence of the relaxation rates. The relaxation rates are shown for (●) the change in fluorescence of the MABA peptide and (■) the change in the near-infrared absorption of the peptide (*1*). The curves are the fast (− −) and slow (−·−) calculated relaxation rates for the decay of the N-terminal helix content and (—) the calculated relaxation rate for the average helix content. The calculation of the relaxation rates is described in the text. The parameters used in the calculation of the kinetics were $s_0 = 1.482$, $\sigma = 0.00117$, $\Delta H_s = -1.3$ kcal/mol residue, and $\Delta H_+ = 0$ kcal/mol residue. The scaled value of k_{+0} was 1.28×10^8 s^{-1}.

tions—helix (*h*) or coil (*c*). A helical residue is considered as one which forms a C═O···H—N hydrogen bond between amino acid *i* and amino acid *i* + 4. The key simplifying assumption in this model is the so-called "single sequence" approximation, in which molecules contain either no helical segments or a single contiguous region of helix. This approximation has been shown to produce equilibrium results that are quite close to those of more complete theories for short peptides (*4*). Kinetically, the simplification introduced by the single sequence approximation is enormous. For a peptide containing $n + 4$ amino acid residues (which can form a maximum of n hydrogen bonds), the number of species is reduced from 2^n to $n(n + 1)/2 + 1$. We consider a sequence that can form 20 such hydrogen bonds. (Our peptide can actually form a maximum of 19 C═O···H—N hydrogen bonds, including the hydrogen bond from the MABA carbonyl at the N-terminus and the hydrogen bond to the amide nitrogen at the C-terminus.) A specific state is specified by the initial and final residue of the helical sequence. A representative configuration is

$$h_1 = 4 \qquad h_f = 17$$
$$ccc\,\boxed{hhhhhhhhhhhhhh}\,ccc \qquad (2)$$

$$chh \underset{k_-}{\overset{k_+}{\rightleftharpoons}} cch \qquad hcc \underset{k_-}{\overset{k_+}{\rightleftharpoons}} hhc$$

The $h \rightarrow c$ and $c \rightarrow h$ reactions can take place at either end with rate constants k_- and k_+, respectively. The ratio k_+/k_- is equal to s, the equilibrium constant for the $hcc \rightarrow hhc$ reaction. The partition function can be straightforwardly evaluated (*2*, *8*):

$$q = 1 + [\sigma s^2/(s-1)^2][s^n + n/s - (n+1)] \qquad (3)$$

The fractional helicity, θ, given by

$$\theta = \frac{1}{q}\sum_{j=1}^{n}(n - j + 1)\sigma s^j \qquad (4)$$

was used to calculate the fit to the CD data in Figure 4c.

All helix⇌coil theories (*2*, *3*, *24*, *54*, *55*) predict that the probability of forming a helical segment in the middle of a peptide sequence is higher than at the termini. This prediction has been confirmed by a variety of experiments (*7*, *56*−*59*). In the single-sequence approximation, this results simply from the fact that the number of positions for the helical sequence which include a given terminal residue, is smaller than the number of positions which include residues closer to the center of the peptide. If we use the fit of the CD data to the single-sequence approximation to predict the helicity of a terminal residue, we find that the maximum probability that the N-terminal residue is helical is significantly smaller than the average helix content, reaching a value of only about 0.4 at 260 K (Figure 4c). Moreover, the dependence of the predicted helix content on temperature is quite similar to that observed for the MABA peptide quantum yield. From this result, we conclude that the MABA fluorescence quantum yield can be considered as a measure of the probability that the carbonyl oxygen forms a backbone hydrogen bond to residue 4 of the peptide.

If we calculate equilibrium distributions of the number of helical residues (n_h) using this approximation, we find that two distinct processes accompany an increase in temperature (Figure 7). The population of molecules that contain a helical sequence redistributes locally along the coordinate which defines the number of helical residues, to produce a distribution with a smaller mean number of helical residues. In addition, the total number of molecules that contain a helical sequence decreases with increasing temperature. When the temperature is jumped in the helix melting

[3] We have assumed a linear temperature dependence of the preexponential factor in the expression for *k*. The temperature dependence of the preexponential factor is a rarely determined quantity in kinetics, and there is only scant information for polypeptides and proteins. For the conformational relaxation rate of a native, mostly helical protein (myoglobin), Ansari *et al*. (*60*) found that at water viscosities ($\eta \approx 1$ cP) the rate is independent of η, while at high η (> 20 cP), the rate varies as η^{-1}, as in Kramers theory for a one-dimensional barrier crossing. Their data were well fit with a preexponential factor proportional to $(\sigma + \eta)^{-1}$, assuming that σ was unchanged over the narrow temperature range of the experiments. Ansari *et al*. interpreted σ (≈4 cP) as the contribution to the total friction from the internal friction of the protein. In the high η limit then, the temperature dependence of the preexponential factor is simply given by the temperature dependence of the viscosity. Klimov and Thirumalai (*61*) have recently performed Langevin simulations of helix formation for a simplified (chain of beads) representation of a polypeptide chain and found that the viscosity dependence of the rate also exhibits one-dimensional Kramers behavior, predicting η^{-1} dependence at water viscosities. These calculations predict that, as the temperature increases over the range of the present experiments (273−340 K), the preexponential factor will increase by a factor of ∼4 because of the decrease in water viscosity (1.8−0.4 cP). However, no internal friction was considered in these simulations, and it is not obvious that it can be ignored. In the absence of any experimental information on the contribution of temperature dependence of the internal friction, we have assumed a simple linear temperature dependence, which only produces an increase in the preexponential factor by a factor of ∼1.2 (= 337/275 K).

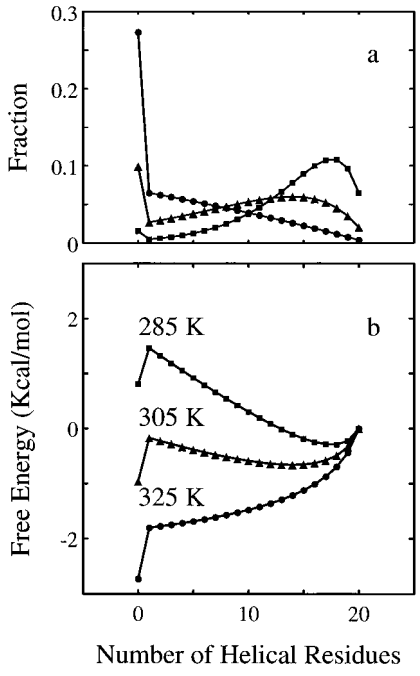

FIGURE 7: Temperature dependence of species populations in the single-sequence approximation. The equilibrium populations at three temperatures are shown as a function of n_h, the number of helical residues.

experiments, these two events are expected to occur on different time scales. The first process, which involves only a few local $h \rightarrow c$ and $c \rightarrow h$ steps, should occur on the time scale of these elementary steps. The second process, which requires that the molecule pass over the free energy barrier at $n_h = 1$, generated by the nucleation step, must be slowed relative to these steps by the height of this barrier. Because the probability of losing the N-terminal H-bond in the first process is relatively high, the MABA fluorescence should change significantly in the more rapid process. Since infrared spectroscopy measures an average helix content, similar to what is expected from CD, it should be more sensitive to the slower global melting step.

To describe the kinetics at this level of approximation, we need only write the differential equations for nucleation and for the motion of the two ends of the helical sequence. If we denote by $\{i,j\}$ the normalized concentration of species in which i is the initial residue of the helical sequence and j is the final residue:

$$\frac{\mathrm{d}\{\text{all coil}\}}{\mathrm{d}t} = -nk_+\sigma\{\text{all coil}\} + k_- \sum_1^n \{i,i\}$$

$$\frac{\mathrm{d}\{i,i\}}{\mathrm{d}t} = k_+\sigma\{\text{all coil}\} + k_-(\{i-1,i\} + \{i,i+1\}) - (2k_+ + k_-)\{i,i\} \quad (5)$$

$$\frac{\mathrm{d}\{i,j\}}{\mathrm{d}t} = k_+(\{i+1,j\} + \{i,j-1\}) + \mathrm{k}_-(\{i-1,j\} + \{i,j+1\}) - 2(k_+ + k_-)\{i,j\}$$

The last two equations describe all cases where $i \neq 1$; $j \neq$ n. When $i = 1$ or $j = n$, the rates which couple $\{i,j\}$ with $\{i-1,j\}$ or $\{i,j+1\}$, respectively, must be set to zero. The average fraction helix is then calculated as

$$\Theta = \frac{1}{n}\sum_{i=1}^{n}\sum_{j=1}^{n}(j-i+1)\{i,j\} \quad (6)$$

and the N-terminal helix content is calculated as

$$\Theta_N = \sum_{j=1}^{n}\{1,j\} \quad (7)$$

We assume that the $c \rightarrow h$ (k_+) and $h \rightarrow c$ (k_-) rates can each be described by the expression $k_x = k_{xo}(T/T_o)\exp(-\Delta H_x^{\ddagger}(T_o - T)/RTT_o)$ where k_{xo} is the rate at the reference temperature ($T_o = 273$ K), T is the temperature, and $\Delta H_x^{\ddagger}$ is the enthalpy of activation. This relation assumes that both the activation enthalpies and activation entropies are temperature independent.[3]

To model the temperature dependence of the measured rates, we must next choose activation enthalpies for k_+ and k_-. We have made the simplifying assumption that the hydrogen bond is fully broken in the transition state and that the activation enthalpy for $h \rightarrow$c is identical to the equilibrium enthalpy change. The activation free energy for c$\rightarrow h$ is therefore purely entropic (but is not necessarily equal to the equilibrium entropy change). With these assumptions we have used the kinetic zipper model to simulate the temporal response to a temperature jump and used the results to calculate the kinetics of the population changes for each of the 211 kinetic species. In modeling the data, a sequence of calculations was carried out at a predetermined set of increasing temperatures. At each temperature, the equilibrium distribution at the preceding temperature was used as the initial condition in calculating the system response. The simulated kinetics for a jump from 285 to 305 K and from 305 to 325 K are shown in Figure 8. The eigenvalues and amplitudes for the jump from 285 to 305 K are shown in Figure 8, panels a and b. The simulated kinetics for the decay in the helix content of the average residue and a terminal residue are shown in Figure 8, panels c and d, respectively. For the average residue, most of the amplitude is associated with the smallest nonzero eigenvalue (Figure 8a) so the simulated kinetics are quite well fitted by a single-exponential relaxation (Figure 8c). For the N-terminus, a cluster of larger eigenvalues produces an additional, more rapid phase (Figure 8b). In this case, the simulated kinetics are well-fitted by the sum of two exponential relaxations (Figure 8d). Importantly, the same result is found at all temperatures, so we shall use this simplified representation of the simulated kinetics in comparing the results from the model with the experimental data.

The fitted rates and amplitudes obtained from a series of simulations throughout the melting curve, using three different sets of values of σ and ΔH_s, are shown in Figure 9. In each case, the values of σ and s_0 were obtained by fitting the equilibrium CD data with an assumed value of ΔH_s. The fitted value of σ is highly dependent on ΔH_s, increasing from about 0.001 to more than 0.04 as ΔH_s decreased from -0.9 to -1.7 kcal/mol residue. The best fits were obtained using values for ΔH_s of -1.3 and -1.5 kcal/mol residue. Scholtz *et al.* (*5*) derived a value of -1.3 kcal/mol residue from scanning calorimetric experiments (with an uncertainty due to difficulties in determining the baseline of about ± 0.45 kcal/mol residue). Schellman (*62*) derived a value of -1.5 kcal/mol residue from the heat of dilution of urea. For each

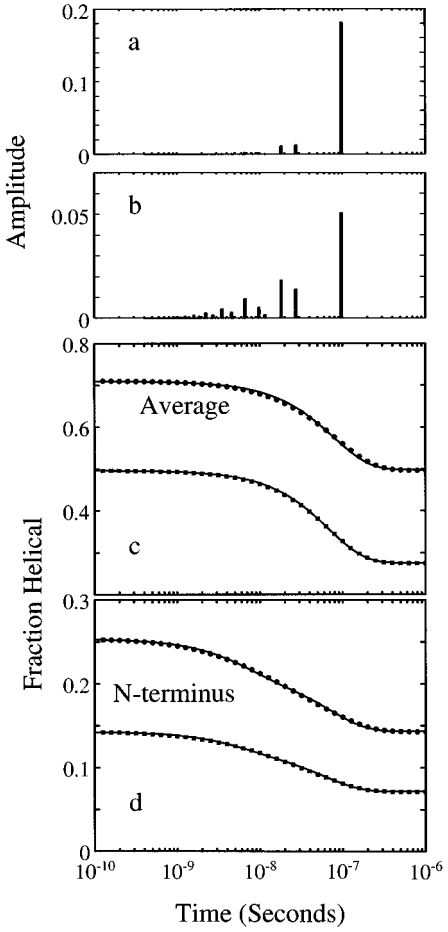

FIGURE 8: Results of kinetic simulations of the helix content using the kinetic zipper model. The kinetics for 20 K temperature jumps were simulated, using the parameters that best fit the equilibrium data of Figure 4. The eigenvalues and amplitudes calculated for a jump from 265 to 285 K are shown for (a) average helix content and (b) N-terminal helix content. The calculated time dependence of the fraction helix for the average residue and the N-terminal residue are shown at final temperatures of 285 and 305 K. (c) Average helix content (●) calculated at 285 K and (■) calculated at 305 K. (—) Fits to the calculated helix content with a single exponential relaxation. (d) N-terminal helix content (●) calculated at 285 K and (■) calculated at 305 K. (—) Fits to the calculated helix content with two exponential relaxations. Parameters are those used in Figure 6, but with $k_{+0} = 3 \times 10^8$ s^{-1}.

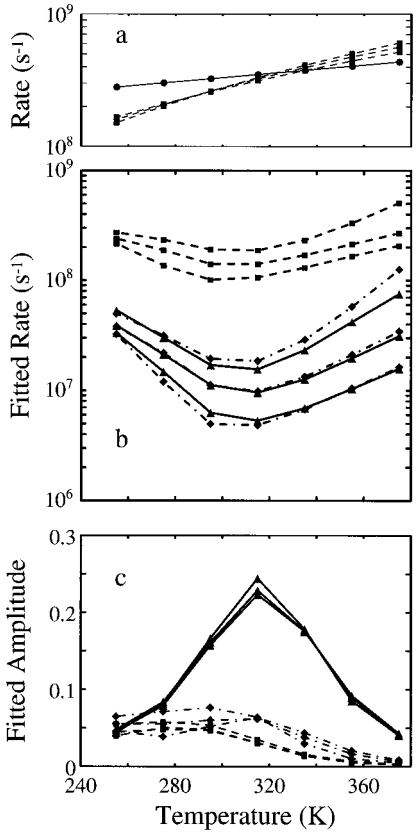

FIGURE 9: Rates and amplitudes obtained from fits to simulations of peptide melting. The results obtained from fits such as those shown in Figure 8 are plotted for three sets of parameters that fit the equilibrium data in Figure 4. (a) Values for k_+ (●) and k_- (■) used in the simulations. The values of the three sets of equilibrium parameters were $\Delta H_s = -0.9$ kcal/mol residue, $\sigma = 0.0017$, and $s_0 = 1.475$; $\Delta H_s = -1.1$ kcal/mol residue, $\sigma = 0.0052$, and $s_0 = 1.46$; $\Delta H_s = -1.5$ kcal/mol residue, $\sigma = 0.025$, and $s_0 = 1.525$. The values of k_{+0} and ΔH_+ were 3×10^8 s^{-1} and 0 kcal/mol residue, respectively. (b) Relaxation rates: (—, ▲) fitted relaxation rates for the average helix content: (– –, ■) fitted relaxation times for the fast component on the N-terminal helix content, (–·–, ♦) fitted relaxation times for the slow component on the N-terminal helix content. For both relaxations, increasing the value of σ increases both relaxation rates, with the slower relaxation rate increasing more. (c) Relaxation amplitudes. The symbols and parameter values are identical to those in panel b. The larger amplitudes for the slow component on the N-terminal helix content at low temperatures (–·–, ♦) are found for larger values of σ.

set of parameter values, the fitted values for the relaxation rates obtained for both the average and N-terminal helix contents exhibit a minimum near the midpoint of the melting transition (Figure 9b). Both of the fitted relaxation rates increase as σ increases, but the increase in the slower relaxation rate is more pronounced. As a result, the ratio of the minimum rates (near the midpoint of the transition) decreases from ~20 to ~10 as σ increases from 0.0017 to 0.06.

The amplitudes predicted by the model are plotted in Figure 9c. The prediction that a probe of the average helix content should exhibit a single exponential is consistent with the IR absorption data. The model also correctly predicts that an N-terminal probe should exhibit a significant amplitude for a more rapid process, as observed for the MABA fluorescence. However, the prediction that the response of a terminal probe should be biphasic, exhibiting comparable amplitudes for both the slow and fast relaxations, is not consistent with our data, which show that the amplitude of a slower relaxation cannot be more than ~10% of the total. At the moment the origin of this inconsistency is not at all clear. One possibility is that the hydrogen bonding properties of the MABA carbonyl differ significantly from those of the amide carbonyl so our model misrepresents the properties of the probe. It is also possible that the present model ignores all sequence dependent features of the peptide and couples the kinetics of the helix terminus too tightly with the average properties of the peptide. Decoupling, either by introducing sequence dependence in helix propensities or by reducing the cooperativity, may result in lower N-terminal amplitudes for the overall melting process.

Using the sets of calculated rates described above, we can adjust the value of k_{+0} at the reference temperature (273 K) and σ to produce relaxation times that optimally match the experimental data. The results of such a limited search are compared with the data in Figure 6. Not only is the model able to explain the minimum in the relaxation rate, but it provides strong support for the argument that the large difference in measured relaxation rates results from the fact

that different properties are being monitored by MABA fluorescence and amide I infrared absorption.

The fundamental $c \rightarrow h$ rate (k_+) required to fit our data is only $1-2 \times 10^8$ s^{-1} (Figure 6). Estimates from relaxation studies on poly-D-glutamic acid and poly-L-glutamic acid in water, where the observed maximum relaxation times are ~ 1 μs, produce similar rates if σ is assumed to have a value of about 10^{-4} (cf. ref 23). The elementary rate for nonionic polymers such as poly-γ-benzyl-L-glutamate in nonaqueous solvents, obtained from earlier relaxation experiments, is significantly faster, about 10^{10} s^{-1} (*14*, *19*, *63*). Gruenewald *et al*. (*23*) have suggested that the $c \rightarrow h$ rate may be slowed in aqueous solvents because hydrogen bonds between water and backbone amide N—H and C═O groups must be broken in order for the residue to access the helical conformation. If the H-bonding activity of the solvent for group i is equal to a, then the effective rate will be given by

$$\langle k_+ \rangle = k_+^0 / \prod_i (1 + K_{ci} a_i) \qquad (8)$$

where k_+^0 is the intrinsic $c \rightarrow h$ rate, and K_{ci} is the effective binding constant of group i for the solvent. If correct, this result has important consequences, since it argues that the approach to the transition state from the coil state is also limited by breaking of water hydrogen bonds. Our results would require that the enthalpy change for this process be close to zero.

Molecular dynamic simulations have also suggested that the $c \rightarrow h$ rate is close to 2 orders of magnitude faster than what we have observed (*12*, *13*). In the study of Daggett and Levitt (*12*) where water was included explicitly, care was taken to ensure that the diffusion constant for water was approximately correct. This argues that water−water hydrogen bonds are parameterized accurately by the potential function. It may, nonetheless, be that water−peptide hydrogen bonds are less accurately parameterized. In the work of Sung and Wu (*13*), water was not included explicitly, so it is not surprising that they overestimate the fundamental $c \rightarrow h$ rate. A second and more interesting possibility for the much larger values obtained from the simulations is that the kinetics for the $h \rightarrow c$ and $c \rightarrow h$ transitions are not exponential, and the rates for these processes exhibit some time dependence. For example, one could imagine that formation of a nascent c state is followed by rapid reversion to the h state before any other kinetic processes occur, perhaps as a result of some 'memory' introduced by the positions of other residues. Given the limitations on the length of the trajectories, the analysis of the dynamics simulations would necessarily focus on the most rapid reactions, whereas the kinetic modeling would reflect the time-averaged rate. Evaluation of these probabilities requires a more complex analysis of significantly longer trajectories than has been carried out to this point.

The value of σ required to match the relaxation times in Figure 6 is approximately 0.01, somewhat larger than 'standard' values that cluster between 0.005 and 0.001. Without this increase, the predicted relaxation time for the average helix content becomes too slow by a factor of about 2. This result is consistent with our fits to the equilibrium data, which also produce relatively large values of σ if ΔH_s is chosen to have its most probable value, suggesting that the cooperativity of short helices has been overestimated in previous studies (*5*, *27*). It is also consistent with the molecular dynamic simulations, which show relatively low cooperativity for the short helices studied (*12*, *13*). The results of our simulations further suggest that kinetic measurements using two different probes may provide a means by which to obtain more accurate values for the nucleation parameter σ. One must err on the side of caution in using the data in Figure 6 to obtain this value. We must acknowledge the fact that the two experiments have not been carried out on the same peptide. Although the existing data suggest that the addition of MABA has little effect on the equilibrium properties of the peptide, we do not yet know to what extent this modification alters its kinetics. Another potential problem is that the single-sequence approximation becomes increasingly worse as the value of σ increases, so it is not possible to use our kinetic model to evaluate σ if its value is significantly greater than ~ 0.003. These problems are not too difficult to overcome. First, it should be straightforward to carry out IR measurements on the labeled peptide; second, the kinetic model can be expanded, for example, by including a second sequence to determine whether the conclusions reached from the limited exploration of helix⇌coil kinetics described here are generally valid.

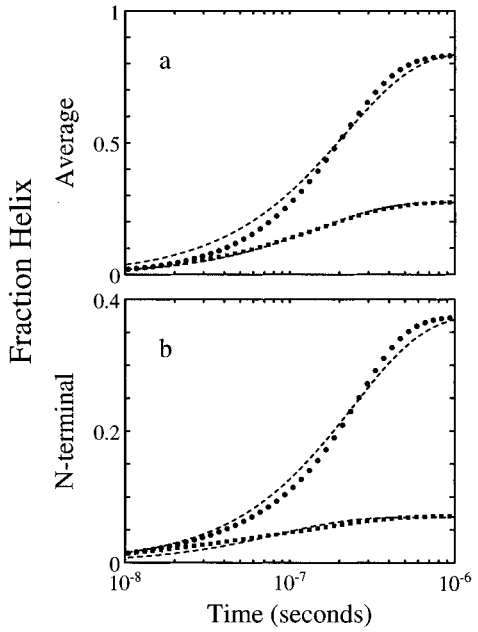

FIGURE 10: Helix formation from the all-coil state. The kinetics of development of the average helix content (a) and the N-terminal helix content (b) predicted by the kinetic zipper model in response to a jump from the all-coil state are shown for final temperatures of 265 and 325K. The fraction helix calculated at (●) 265 K and (■) 325 K shown, together with (---) exponential fits to data. The relaxation times for the exponential curves in (a) are 216 ns at 265 K and 146 ns at 325 K. The relaxation times for the exponential curves in (b) are 242 ns at 265 K and 86 ns at 325 K. The parameter values used in the simulations are given in the legend to Figure 6.

What is the origin of the complex temperature dependence seen in both the MABA fluorescence data and in the kinetics predicted by the kinetic zipper model? The simulations show that the slow relaxation results from equilibration of the time-averaged distribution of species that contain helical sequences with the all-coil state. Moreover, no fast relaxation is predicted for either the average helical residue or the N-terminal residue when all-coil initial conditions are used for the simulation (see Figure 10). Since the distribution of helix-containing species equilibrates faster than the time

required to cross the nucleation barrier, it should be possible to treat the kinetics for this relaxation using a two-state model similar to that used for protein folding (*64*). At 305 K this barrier is higher than both the all-coil state and the populated helical states (Figure 7b). At low temperature, the height of this barrier relative to the all coil state decreases and the probability of proceeding from the barrier toward helix-containing states also increases. These effects dominate the very small temperature dependence of k_+, so the overall coil→helix rate increases with decreasing temperature. At high temperatures, the barrier between the helix-containing states disappears, accelerating the helix→coil rate. Because the faster of the overall helix→coil (k_{hc}) and coil→helix (k_{ch}) rates dominates the observed relaxation rate, ($k_{hc} + k_{ch}$), it exhibits a *minimum* near the midpoint of the folding curve and *increases* at both low and high temperatures.

The origin of the weak minimum observed for the faster relaxation rate is less obvious. A minimum in the fitted rates is observed for all sets of parameter values used in calculating the relaxation times in Figure 9b, despite the fact that both k_+ and k_- are increasing with increasing temperature (Figure 9a). The principal effect of parameter values on the rate of the fast relaxation is to shift the minimum to slightly lower temperatures as ΔH_s becomes more negative, a result which can be explained by the fact that k_- becomes more temperature dependent. The fact that both k_+ and k_- are 2−3 times larger than the minimum rate of the fast relaxation, observed at ∼300 K, but become comparable to the maximum rates observed at low temperatures provides a clue to the source of the observed temperature dependence. These facts, together with Figure 8, which shows that a cluster of similar eigenvalues contribute to the amplitude of this relaxation, suggest that it corresponds to a diffusion-like process in which the helix-containing species re-equilibrate to the change in temperature. At low temperatures the length of the helical sequence is close to its maximum value of n. The temperature jump induces only small changes in the average number of helical residues, and the observed relaxation time is close to the single step relaxation time $(k_+ + k_-)^{-1}$. Near the midpoint of the transition, a number of sequential steps are required to go from the initial to the final distribution of helical sequence lengths, so the rate becomes significantly slower than the single step relaxation time. The increased 'distance' that the population must traverse to equilibrate appears to be responsible for producing the minimum in the measured rate. At temperatures above the midpoint, three effects act to increase the rate: first, the single step relaxation times decrease because of the temperature dependence of both k_+ and k_-; second, the free energy surface is biased so that the population of helix-containing states is moving 'downhill'; third, the number of residues in the average helical sequence is decreasing (Figure 7), thereby decreasing the number of $h \rightarrow c$ and $c \rightarrow h$ steps required to reach equilibrium.

All of the simulations described to this point model the response to a temperature increase, so there is little or no contribution to the observed kinetics from helix formation from the all-coil state. The kinetics of helix formation are of intrinsic interest both in the folding of proteins and in interpreting the results of dynamics simulations. In Figure 10, we present the coil→helix kinetics calculated using the kinetic zipper model for two final temperatures. The kinetics for the average helix content are less well approximated by a single-exponential relaxation than those in Figure 8, particularly at 265 K where the helix is very stable. The appearance of helix shows detectable temporal cooperativity, presumably because the time required for the development of the average properties of the helix-containing species is comparable to the reciprocal of the nucleation rate. At the higher temperature, where the average length of the helical segment is shorter, the kinetics are more nearly exponential. Similar behavior is observed for the N-terminal helix content. The cooperative time courses arise from the interplay of the same two processes (nucleation and redistribution of helix lengths) discussed above but, when starting from the all-coil state, the slower nucleation step must occur first. Redistribution of the helix-containing species is also somewhat slower because it now begins with only a single helical residue in the peptide. Because the rates for the two processes are more similar, the slow relaxation becomes non-exponential.

CONCLUDING REMARKS

The results of our experiments, which provide the first direct observation of the rate of helix propagation, show that this rate is relatively slow ($\sim 10^8$ s^{-1}). They further show that the relaxation rate for redistribution of helix lengths is nearly temperature independent, exhibiting a minimum near the midpoint of the melting transition. The rates observed for an N-terminal probe are significantly faster than those observed for the average peptide residue by infrared absorption measurements (*1*). The kinetic zipper model, together with a relatively simple picture in which the temperature-dependence of the $c \rightarrow h$ propagation rate is minimized, provides a consistent explanation of all three results but also predicts that the N-terminal probe should exhibit a significant amplitude for the slower process, which we do not observe. Our results further suggest that it may be possible to accurately assess helix cooperativity, represented in our model by the value of σ, by comparing the relaxation rates for helix⇌coil kinetics probed by an end label, such as our fluorescence probe, and by a bulk label, such as circular dichroism or infrared absorption.

ACKNOWLEDGMENT

We are indebted to Peter Kim, who not only suggested that we study the MABA-labeled peptide but also generously supplied us with all of the material used in this work. We would also like to thank Robert W. Zwanzig for discussions that led to the implementation of the kinetic zipper model.

REFERENCES

1. Williams, S., Causgrove, T. P., Gilmanshin, R., Fang, K. S., Callender, R. H., Woodruff, W. H., and Dyer, R. B. (1996) *Biochemistry 35*, 691−697.
2. Schellman, J. A. (1958) *J. Phys. Chem. 62*, 1485−1494.
3. Zimm, B. H., and Bragg, J. K. (1959) *J. Chem. Phys. 31*, 526−535.
4. Qian, H., and Schellman, J. A. (1992) *J. Phys. Chem. 96*, 3987−3994.
5. Scholtz, J. M., Marqusee, S., Baldwin, R. L., York, E. J., Stewart, J. M., Santoro, M., and Bolen, D. W. (1991) *Proc. Natl. Acad. Sci. U.S.A. 88*, 2854−2858.
6. Chakrabartty, A., Schellman, J. A., and Baldwin, R. L. (1991) *Nature 351*, 586−588.

7. Scholtz, J. M., and Baldwin, R. L. (1992) *Annu. Rev. Biophys. Biomol. Struct. 21*, 95−118.
8. Cantor, C. R., and Schimmel, P. R. (1980) in *Biophysical Chemistry, Part III*, W. H. Freeman, San Francisco, CA.
9. Schwarz, G. (1965) *J. Mol. Biol. 11*, 64−77.
10. Soman, K. V., Karimi, A., and Case, D. A. (1991) *Biopolymers 31*, 1351−1361.
11. Daggett, V., Kollman, P. A., and Kuntz, I. D. (1991) *Biopolymers 31*, 1115−1134.
12. Daggett, V., and Levitt, M. (1992) *J. Mol. Biol. 223*, 1121−1138.
13. Sung, S.-S., and Wu, X.-W. (1996) *Proteins: Struct., Funct., Genet. 25*, 202−214.
14. Schwarz, G., and Seelig, J. (1968) *Biopolymers 6*, 1263−1277.
15. Burke, J. J., Hammes, G. G., and Lewis, T. B. (1965) *J. Chem. Phys. 42*, 3520−3525.
16. Parker, R., Slutsky, L., and Applegate, K. (1968) *J. Phys. Chem. 72*, 3177−3186.
17. Hammes, G. G., and Roberts, P. B. (1969) *J. Am. Chem. Soc. 91*, 1812−1817.
18. Barksdale, A., and Stuehr, J. (1972) *J. Am. Chem. Soc. 94*, 3334−3338.
19. Wada, A., Tanaka, T., and Kihara, H. (1972) *Biopolymers 11*, 587−605.
20. Sano, T., Yasunaga, T., Tsuji, Y., and Ushio, H. (1975) *Chem. Instrum. 6*, 285−296.
21. Cummins, A. L., and Eyring, E. M. (1975) *Biopolymers 14*, 2107−2114.
22. Tsuji, Y., Yasunaga, T., Sano, T., and Ushio, H. (1976) *J. Am. Chem. Soc. 98*, 813−818.
23. Gruenewald, B., Nicola, C. U., Lustig, A., Schwarz, G., and Klump, H. (1979) *Biophys. Chem. 9*, 137−147.
24. Poland, D., and Scheraga, H. A. (1966) *J. Chem. Phys. 45*, 2071−2090.
25. McQuarrie, D. A., McTague, J. P., and Reiss, H. (1965) *Biopolymers 3*, 657−663.
26. Gō, N. (1967) *J. Phys. Soc. Jpn. 22*, 416−427.
27. Munoz, V., and Serrano, L. (1995) *Curr. Opin. Biotechnol. 6*, 382−386.
28. Thompson, P. A., Eaton, W. A., and Hofrichter, J. (1996) *Protein Sci. 5*, 67.
29. Thompson, P. A. (1997) in *Techniques in Protein Chemistry, VIII* (Marshak, D. R., Ed.) Academic Press, San Diego, CA.
30. Gilmanshin, R., Williams, S., Callender, R. H., Woodruff, W. H., and Dyer, R. B. (1997) *Proc. Natl. Acad. Sci. U.S.A. 94*, 3709−3713.
31. Ballew, R. M., Sabelko, J., and Gruebele, M. (1996) *Proc. Natl. Acad. Sci. U.S.A. 93*, 5759−5764.
32. Phillips, C. M., Mizutani, Y., and Hochstrasser, R. M. (1995) *Proc. Natl. Acad. Sci. U.S.A. 92*, 7292−7296.
33. Brooks, C. L., and Case, D. A. (1993) *Chem. Rev. 93*, 2487−2502.
34. Doig. A. J., Chakrabartty, A., Klinger, T. M., and Baldwin, R. L. (1994) *Biochemistry 33*, 3396−3403.
35. Padmanaban, S., and Baldwin, R. L. (1994) *J. Mol. Biol. 237*, 500−512.
36. Staerk, H., and Czerlinski, G. (1965) *Nature 205*, 63−64.
37. Hoffmann, H., Yeager, E., and Stuehr, J. (1968) *Rev. Sci. Instrum. 39*, 649−653.
38. Beitz, J. V., Flynn, G. W., Turner, D. H., and Sutin, N. (1970) *J. Am. Chem. Soc. 92*, 4130−4132.
39. Turner, D. H., Flynn, G. W., Sutin, N., and Beitz, J. V. (1972) *J. Am. Chem. Soc. 94*, 1554−1559.
40. Williams, A. P., Longfellow, C. E., Freier, S. M., Kierzek, R., and Turner, D. H. (1989) *Biochemistry 28*, 4283−4291.
41. Young, W. S., and Brooks, C. L. (1996) *J. Mol. Biol. 259*, 560−572.
42. Brooks, C. L. (1996) *J. Phys. Chem. 100*, 2546−2549.
43. Lockhart, D. J., and Kim, P. S. (1992) *Science 257*, 947−951.
44. Goodall, D. M., and Greenhow, R. C. (1971) *Chem. Phys. Lett. 9*, 583−586.
45. Anfinrud, P. A., Han, C., and Hochstrasser, R. M. (1989) *Proc. Natl. Acad. Sci. U.S.A. 86*, 8387−8391.
46. Cowgill, R. W. (1968) *Biochim. Biophys. Acta 168*, 431−438.
47. Shoemaker, K. R., Kim, P. S., York, E. J., Stewart, J. M., and Baldwin, R. L. (1987) *Nature 326*, 563−567.
48. Scholtz, J. M., Qian, H., York, E. J., Stewart, J. M., and Baldwin, R. L. (1991) *Biopolymers 31*, 1463−1470.
49. Chen, T.-H., Yang, J. T., and Chau, K. H. (1974) *Biochemistry 13*, 3350−3359.
50. Madison, V., and Schellman, J. (1972) *Biopolymers 11*, 1041−1076.
51. Feitelson, J. (1964) *J. Phys Chem. 68*, 931−397.
52. Cowgill, R. W. (1967) *Biochim. Biophys. Acta 133*, 6−18.
53. Cowgill, R. W. (1968) *Biochim. Biophys. Acta 168*, 417−430.
54. Lifson, S., and Roig, A. (1961) *J. Chem. Phys. 34*, 1963−1974.
55. Poland, D., and Scheraga, H. A. (1970) in *Theory of Helix−Coil Transitions in Biopolymers*, Academic Press, New York.
56. Bradley, E. K., Thomason, J. F., Cohen, F. E., Kosen, P. A., and Kuntz, I. D. (1990) *J. Mol. Biol. 215*, 607−622.
57. Miick, S. M., Todd, A. P., and Millhauser, G. L. (1991) *Biochemistry 30*, 9498−9503.
58. Liff, M. I., Lyu, P. C., and Kallenbach, N. R. (1991) *J. Am. Chem. Soc. 113*, 1014−1019.
59. Rohl, C. A., and Baldwin, R. L. (1994) *Biochemistry 33*, 7760−7767.
60. Ansari, A., Jones, C. M., Henry, E. R., Hofrichter, J., and Eaton, W. A. (1992) *Science 256*, 1796−1798.
61. Klimov, D. K., and Thirumalai, D. *Phys. Rev. Lett.* (in press).
62. Schellman, J. A. (1955) *Comp. Rend. Trav. Lab. Carlsberg. Ser. Chim. 29*, 223−229.
63. Wada, A. (1971) *Chem. Phys. Lett. 8*, 211−213.
64. Zwanzig, R. W. (1997) *Proc. Natl. Acad. Sci. U.S.A. 94*, 148−150.

BI9704764